Accessing molecular memory *via* a disulfide switch†

Andrew C. Benniston,* Ben D. Allen, Anthony Harriman,* Irantzu Llarena, James P. Rostron and Beverly Stewart

Received 22nd August 2008, Accepted 17th October 2008
First published as an Advance Article on the web 24th November 2008
DOI: 10.1039/b814676d

Herein we describe the results of a combined theoretical and spectroscopic investigation into the design of a simple molecular system intended to act as a memory storage bank. The main operating principle revolves around the two-electron reduction of an aryl disulfide bond. Addition of the first electron leads to elongation of the S–S bond but it breaks only if there is accompanying protonation. Adding a second electron causes S–S bond cleavage, with or without protonation. The structural changes have been assessed by way of quantum chemical calculations and molecular dynamics simulations. Electrochemical studies show that the two-electron reduced product can be re-oxidised at mildly anodic potentials and the cycle can be repeated many times. Both theory and experiment point towards pronounced potential inversion whereby the second reduction potential lies at a significantly more positive potential than that for the first step. Computer simulations of the cyclic voltammograms give rise to numerical values for the reduction potentials that are in quite good agreement with the computed values and also allow determination of the electrochemical rate constants and transfer coefficients. Accurate simulation of the experimental data can be realised only if one proton accompanies the second reduction step. The possibility to design an effective molecular-scale memory device around this system is discussed briefly.

Introduction

The miniaturisation of integrated circuits is set to reach its inherent limitation within the next two decades or so, when current technologies cannot be scaled down any further. Before that time, attention must swing toward the field of molecular electronics and, in particular, to the development of DRAMs (*i.e.*, dynamic random access memories)[1] to be used in conjunction with molecular-scale wires[2] in defect-tolerant architectures.[3] A few error-tolerant memory circuits have already been realised[4] but research is still at the stage of identifying possible materials for use as ultra-dense molecular memories.[5] An obvious problem related to the use of molecular components for such purposes is the need to ensure that the storage process remains non-volatile (*i.e.*, data are not lost if the power is cut). Although several different types of molecular memory systems have been suggested,[6] those based on a redox-enforced conformational change seem to be the most viable.[7] Here, charge is stored at a redox-active site by way of an electrochemical reaction that can be reversed on application of a different bias potential. The electrode process is complemented by a large change in geometry such that vastly disparate reduction potentials are found for the forward and reverse steps.[8] In principle, a molecular material should allow for a far greater capacitance per unit area than can be achieved with conventional DRAM memory but this situation has yet to be achieved in a practical manner.

In searching for molecules that might function in the desired way we have examined the electrochemical properties of 3,8-diiodo-dibenzo[1,2]dithiine, **1** (Fig. 1). This candidate has been selected for detailed study because it is well known that disulfides undergo bond cleavage upon two-electron reduction to give a pair of thiolate anions.[9] This compound is interesting as a molecular memory medium, not least because of its relatively small mass and facile synthesis that favour its easy integration into more complex architectures.[10] Moreover, unlike simpler analogues[9] such as diphenyldisulfide, **1** cannot dissociate upon reduction but is still able to undergo internal twisting so as to minimise electrostatic repulsion between the resultant thiolate centres. This provides the basis for a concerted electron transfer and structural change that might be exploitable for the design of a data storage device.[10,11] It also raises questions about the mechanism for the electrochemical processes,[11] and this forms the basis of the present investigation.

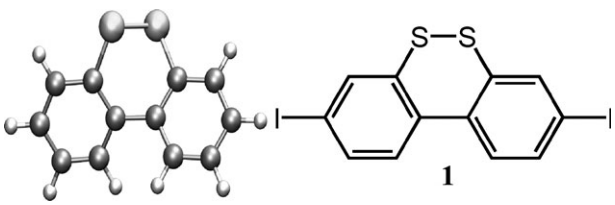

Fig. 1 Molecular formulae and the energy-minimised structure computed for 3,8-diiodo-dibenzo[1,2]dithiine, **1**.

Molecular Photonics Laboratory, School of Chemistry, Newcastle University, Newcastle upon Tyne, UK NE1 7RU.
E-mail: a.c.benniston@ncl.ac.uk.
E-mail: anthony.harriman@ncl.ac.uk; Fax: +44 (0)191 222 6929; Tel: +44 (0)191 222 5706

† Dedicated to Prof. Jean-Pierre Sauvage on the occasion of his 65th birthday.

Results and discussion

A preliminary communication[10] described the synthesis of **1** starting from 4,4′-diiodobiphenyl-2,2′-diol. The full synthetic details are to be found in the Experimental section. The title compound was purified by extensive column chromatography on silica gel using petroleum ether–diethyl ether (3 : 1) as eluent, followed by recrystallisation from hot $CHCl_3$. The overall structure of the compound was confirmed by single-crystal X-ray crystallography, as reported previously.[10]

Cyclic voltammetric reduction of 1

The energy-minimised structure of 3,8-diiododibenzo-[1,2]dithiine, **1**, calculated at the Hartree–Fock 3-21G* level, is displayed in Fig. 1 and, in agreement with the crystal structure,[10] shows the molecule to be slightly twisted around the central axis so as to accommodate the disulfide linkage. Indeed, the computed dihedral angle for the inter-ring connection is 34°, while the S–S bond length is calculated to be 2.055 Å. Considerable electron density is localised on the sulfur atoms (Fig. 2) and this introduces a modest dipole moment of 3.6 D, as computed at the CNDO level. The terminal iodine atoms are present as a simple means by which to facilitate coupling to other molecules. It was found that **1** dissolved readily in a variety of common organic solvents although saturation was easily achieved. The compound was stable over prolonged storage and was found to be non-fluorescent. A reasonably intense absorption band is evident at around 305 nm in dichloromethane solution and can be assigned to a π–π* transition. There is a weak shoulder centred at *ca.* 327 nm that might be due to the n–π* transition associated with the sulfur atoms, while a more intense π–π* transition is located at around 220 nm. The expected σ–σ* transition due to the disulfide bond cannot be resolved from the more intense π–π* bands, and it was notable that solutions of the compound were stable on exposure to room light.

Cyclic voltammetry studies were conducted with **1** in deoxygenated CH_2Cl_2 at room temperature. Attempts to measure cyclic voltammograms in the presence of acid afforded irreproducible results. On cathodic scans, a peak is observed at about −1.5 V *vs.* SCE. This peak is electrochemically irreversible and is assigned to reduction of the disulfide bond on the basis that quantum chemical calculations locate the LUMO as residing on this bond. It is also notable that the electrochemical behaviour is similar to that described for diphenyldisulfide.[9] The peak potential, E_P, becomes more negative as

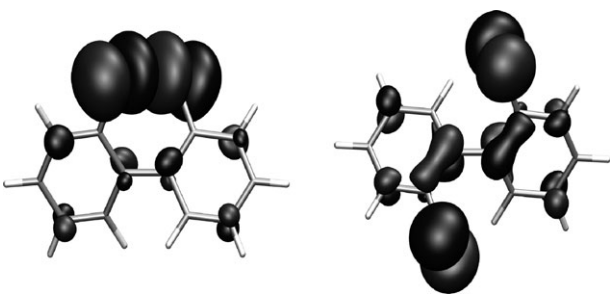

Fig. 2 Computed electron-density distribution for the LUMO of **1** (left hand side) and the corresponding dithiolate (right hand side).

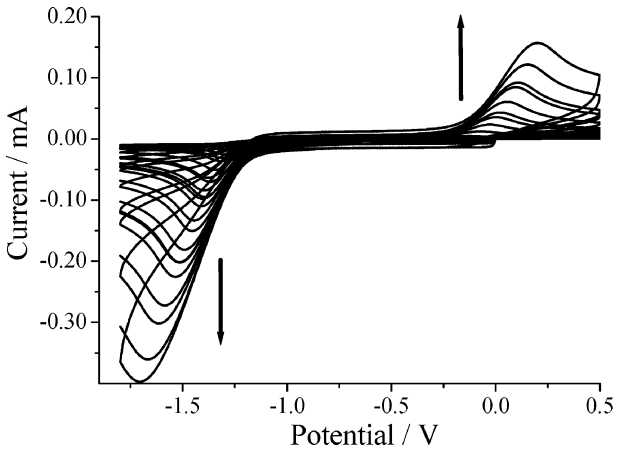

Fig. 3 Cyclic voltammograms recorded for the reduction of **1** in CH_2Cl_2 containing background electrolyte. Sweep rates increased progressively from 50 mV s^{-1} to 2 V s^{-1}.

the scan rate increases (Fig. 3) while the peak current, i_P, increases linearly with the square root of the scan rate, υ (Fig. 4). Linear correlations were also observed between E_P and $\ln(i_P)$, between E_P and $\upsilon^{1/2}$, and between $\ln(\upsilon)$ and E_P, at least over limited scan rates (Fig. 4). Chrono-amperometric experiments[12] were performed with a microelectrode for various initial concentrations of **1** and analysed in terms of the Shoup and Szabo approach (Fig. 5).[13] Fitting the curve over the entire time range allowed calculation of the total number of electrons transferred during the electrochemical reaction ($n = 2$), and of the diffusion coefficient ($D = 1.5 \pm 0.2 \times 10^{-6}$ cm^2 s^{-1}) for the electrode-active species. Earlier work has already shown that the electrochemical reduction of simpler aryl disulfides[9] involves a two-electron process. Using these derived values in the Butler–Volmer equation[11] allows calculation of the transfer coefficient for the cathodic step, α_C, as being 0.70 ± 0.06. At slow scan rates, there is no obvious sign of any other electrode-active species in the voltammograms, but at higher scan rates an anodic process can be seen around 0 V *vs.* SCE. This latter process is not apparent unless the potential has first been swept in a cathodic direction. As such, the anodic wave corresponds to the oxidation of a product formed during reduction. At extreme potentials, the two iodine atoms are oxidized at *ca.* 1.7 V *vs.* SCE and reduced at *ca.* −2.0 V *vs.* SCE. Each of these latter processes involves the transfer of two electrons and is electrochemically irreversible.

Even at a fast scan rate, the ratio of peak currents for the anodic and cathodic steps does not exceed *ca.* 60%, except at low temperature. This situation arises because the large potential separation between cathodic and anodic peaks allows the reduction product to diffuse from the electrode surface before re-oxidation can take place. This separation of the cathodic and anodic peaks, which varies from 1.06 V at a sweep rate of 50 mV s^{-1} to 1.91 V at a sweep rate of 2 V s^{-1}, implies slow electrode kinetics.[11] Analysis of the re-oxidation step gave rise to a transfer coefficient, α_A, of 0.44 ± 0.05. The sum of α_C and α_A ($= 1.14$) can be used to suggest that the rate-determining reaction involves only a single electron.[14] Furthermore, the observation that two electrons are involved in the cathodic reaction but only one electron is transferred in

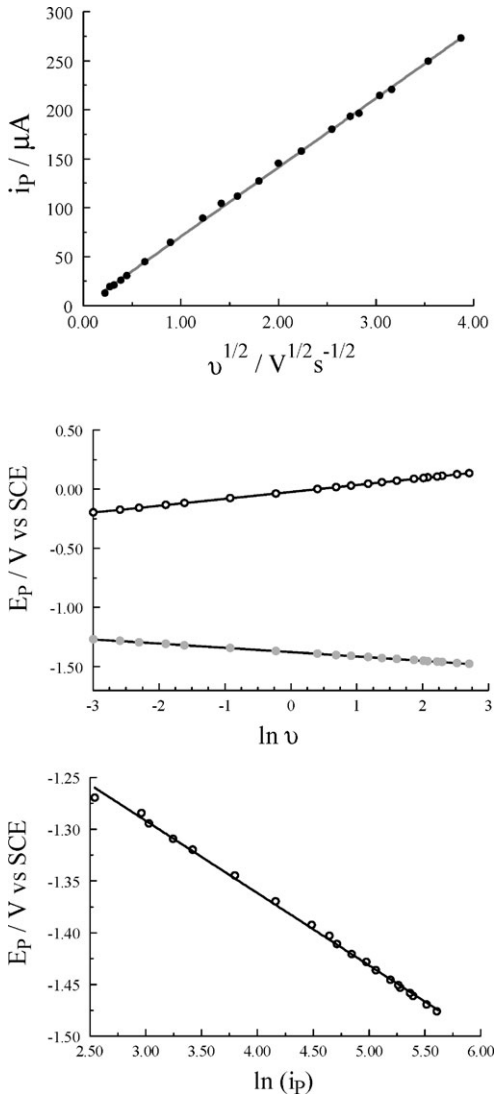

Fig. 4 Plots showing the variation of peak current with square root of scan rate (top panel), peak potential (E_p) with ln(υ) (middle panel) and peak potential (E_p) and ln(i_p) (bottom panel).

the rate-determining step points to a multi-step electrochemical reaction rather than a concerted two-electron change.[15]

A critical feature of any putative molecular memory device is that the chemical reactions are fully reversible and that all species involved in the electrochemical processes are chemically stable. The slow electrode kinetics inferred from the shape of the cyclic voltammograms allow any inherent chemical steps, such as disproportionation, to compete and it is important to assess the likelihood of any such reactions. In fact, the ratio of the diffusion-controlled currents (i_D) from the chronoamperometric response and the ratio of diffusion-controlled charges (c_D) from the chronocoulometric response are usually taken to be characteristic of the chemical stability and reversibility of a redox couple.[11] The theoretical value for i_D is 0.293 and remarkably close to the experimental value of 0.294. Likewise the experimental (c_D = 0.412) and theoretical (c_D = 0.414) charges are in excellent agreement. This behaviour confirms the high chemical stability of the system and holds promise for the development of a fatigue-resistant molecular memory.

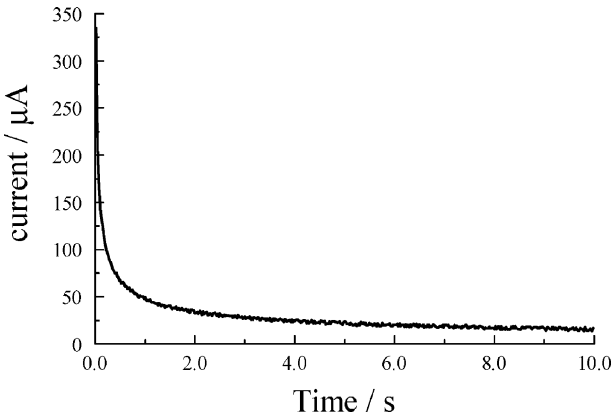

Fig. 5 Plot from chrono-amperometric experiments showing the variation of current with time.

Spectro-electrochemistry

Compound **1** was dissolved in anhydrous, deoxygenated CH_2Cl_2 (1.2 mM) containing 0.2 M tetra-*N*-butylammonium tetrafluoroborate as background electrolyte and studied by spectro-electrochemistry. Thus, electrochemical reduction at −1.5 V *vs.* SCE caused the progressive transformation of **1** into a stable product. The reaction was easily followed by UV-visible absorption spectroscopy, as shown in Fig. 6; the absorption band centred at 305 nm is replaced by a new band centred at 275 nm, and there is a clear isosbestic point at 292 nm. Electrolysis at −1.9 V *vs.* SCE has the effect of converting this product into a second species that absorbs around 240 nm but also shows increased absorbance at about 350 nm. A clear isosbestic point is seen at 255 nm but the isosbestic point around 308 nm is not fully preserved during electrolysis, possibly because of partial precipitation of the final product. Nonetheless, two stable products are seen that differ by their respective reduction potentials. The reaction was also followed by FT-IR spectroscopy but little structural information was provided by these particular experiments.

The second electrochemical process observed in the spectro-electrochemical studies corresponds to reduction of the

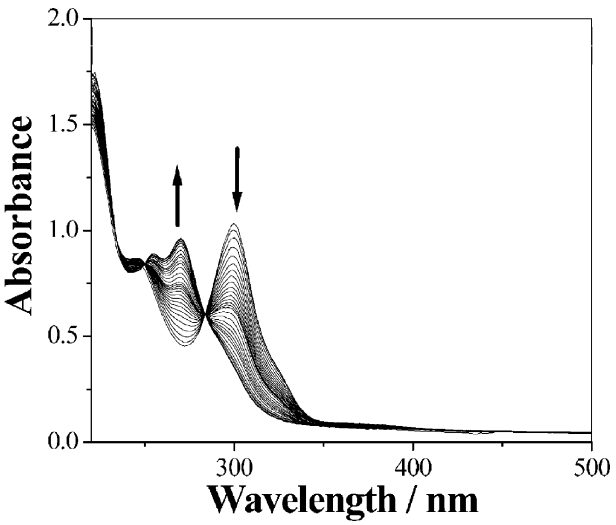

Fig. 6 Spectro-electrochemical studies carried out with **1** in deoxygenated CH_2Cl_2 solution with an applied potential of −1.5 V *vs.* SCE.

iodobenzene moiety and is an artefact of the system selected for study. The first process is the one of interest here since it refers to the switching action. This is a two-electron reaction and, on the basis of studies made earlier with simpler aryl disulfides,[9] can be assigned to reduction of the disulfide bond. The resulting product will be the dithiolate, although there might be partial protonation if trace amounts of water are present. Computer modelling studies indicate that the two-electron reduction of **1** will be accompanied by a substantial geometry change in order to minimise electrostatic repulsion and stereochemical effects. Indeed, the energy-minimised geometry for the dithiolate has an inter-ring dihedral angle of 130° and an S–S separation distance of *ca.* 5.35 Å. The dithiolate is considerably less stable than the starting disulfide, in both a vacuum and a polar solvent. The computational studies indicate that the HOMO has significant electron density on the sulfur centre. The dithiolate is re-oxidised at potentials of around 0 V *vs.* SCE, without overall loss of material, and it is also important to note that EPR studies failed to detect the presence of free radicals, as might arise from the one-electron reduction of **1** to the corresponding π-radical anion. Thus, comproportionation of the dithiolate seems to be unimportant under these experimental conditions.

Electrochemical mechanism

The system under investigation corresponds to the two-electron inter-conversion between the disulfide and the corresponding dithiolate species. There is a substantial change in geometry and the electrochemical steps appear to be kinetically slow. The structural change involves dissociation–reformation of the disulfide bond and rotation around the connecting C–C bond, at least according to computational studies (see later). Once the disulfide bond is broken, internal rotation is facile and is likely to be relatively fast. Indeed, no intermediate species could be detected by electrochemical methods and this raises the possibility that the overall reaction involves concerted electron transfer and geometry change. Given that the electron-transfer chemistry is fully reversible, the reaction can be considered in terms of Scheme 1, with due allowance for the fact that only a single geometry is available to the initial disulfide (S). Within this scheme, addition of the first electron results in formation of the corresponding π-radical anion ($S^{-\bullet}$). This species can accept a second electron to form the dianion (S^{2-}) before a change in geometry takes place, or rearrange to a new energy-minimised structure ($R^{-\bullet}$) prior to addition of the second electron. Consequently, the resultant dianion must undergo further structural re-arrangement to the preferred geometry computed for the dithiolate (T^{2-}). Alternatively, bond dissociation could take place at the π-radical anion stage, forming $T^{-\bullet}$, and be followed by addition of the second electron without a substantial change in geometry. The possibility for potential inversion exists for all routes.[16,28] As a final complication, it is necessary to consider the effects of protonation of the reduced species, even though our experimental studies are made in acetonitrile, and the relevant species are added in parenthesis to Scheme 1. It is implausible that S will be protonated under any conditions, the quantum chemical studies strongly support this intuitive notion by giving a calculated pK_A in acetonitrile of −25.5, and such species have been eliminated from Scheme 1. There is more likelihood of the π-radical anion and dianion becoming protonated and this possibility was examined in depth by quantum chemical calculations.

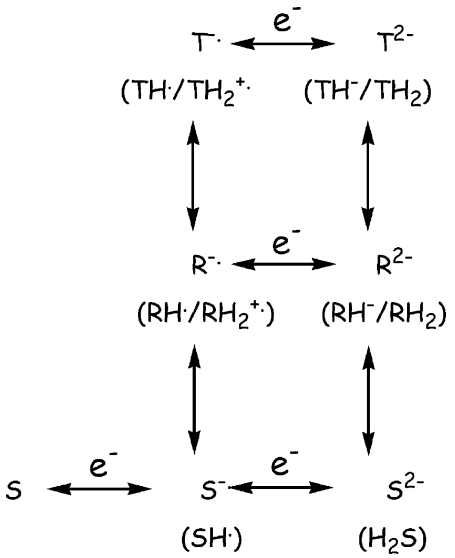

Scheme 1 Proposed sequence of events associated with the reversible 2-electron reduction of the disulfide **1** and allowing for the change in geometry. The left–right direction represents the electron-transfer steps whereas the up–down direction refers to stepwise changes in geometry.

Quantum chemical studies

Unravelling the detailed reaction mechanism is not possible on the basis of the results discussed so far, but additional insight can be gained by quantum chemical studies. The calculations were performed in simulated dichloromethane (CH_2Cl_2) and acetonitrile (CH_3CN), both of which are widely used in electrochemical experiments, and *in vacuo*. Solvent effects are expected to play a crucial role in determining both reduction potentials and protonation states, and have been included in the calculations using the integral equation formalism polarisable continuum model (IEFPCM).[17] Table 1 contains selected geometric parameters of the minimum energy structures for all species, for both gas-phase and solvated systems. Species are labelled according to the number of excess protons and electrons they possess, relative to the initial starting material, S. The bond length between phenyl units (C–C) is reported, as well as the separation between sulfur atoms (S–S), and the torsion angle between the plane of the phenyl rings. In general, reduction of S leads to a lengthening of the central C–C bond, while protonation of one or both S atoms shortens it. For $R^{-\bullet}$, the dihedral angle, and hence the S–S separation, increases in keeping with the population of the σ* orbital located on the sulfur bridge. However, the occupation of the anti-bonding orbital is insufficient in itself to break the bridge. For the protonated species $RH^{\bullet}$, a significant increase in the dihedral angle accompanies reduction, so that the phenyl rings become almost perpendicular. This extreme change in geometry indicates that the bridge has been broken, with the excess electron being localised on the non-protonated sulfur atom. This is confirmed by examination of the spin density

Table 1 Geometric parameters of the various structures determined at the B3LYP/6-31++G** level

	C–C/Å			S–S/Å			Dihedral angle/°		
Species	Gas	CH_2Cl_2	CH_3CN	Gas	CH_2Cl_2	CH_3CN	Gas	CH_2Cl_2	CH_3CN
S	1.49	1.49	1.49	2.10	2.10	2.10	33	33	33
HS^+	1.49	1.50	1.50	2.11	2.11	2.11	31	31	31
H_2S^{2+}	1.49	1.49	1.49	2.46	2.43	2.43	38	37	37
$R^{-\bullet}$	1.49	1.49	1.49	2.77	2.78	2.79	49	49	49
$RH^\bullet$	1.49	1.50	1.50	4.73	4.19	4.12	110	90	87
$RH_2^{+\bullet}$	1.47	1.47	1.47	4.87	4.94	4.94	128	131	131
T^{2-}	1.50	1.50	1.50	5.51	5.38	5.35	134	131	130
TH^-	1.50	1.50	1.59	3.34	3.37	3.38	63	64	64
TH_2	1.50	1.50	1.50	4.40	4.40	4.40	102	102	102

resident on each sulfur atom, which shows the protonated atom having a Mulliken spin density of 0 electrons, while the non-protonated sulfur atom has a spin density of 0.7 electrons. This can be compared with the equivalent spin densities found in $R^{-\bullet}$, where each sulfur atom has 0.48 electrons. The second reduction step has the effect of breaking the S–S bond for both non-protonated (T^{2-}) and doubly-protonated (TH_2) species. However, the geometry of the singly-protonated species (TH^-) is interesting since the single proton orients between the two sulfur atoms, effectively reforming the bridge that was broken during the first reduction step.

To calculate the reduction potentials for each step in Scheme 1, we have adopted the method used by Holland *et al.*[18] in determining reduction potentials for a series of organocopper complexes. Their method removes the need for explicit determination of solvated vibrational frequencies, and provides results accurate to a few tenths of a volt across a range of compounds. The IEFPCM method, as used to model the solvent interactions in the present study, is unsuitable for the determination of vibrational frequencies (and hence absolute free energies) for two reasons. Firstly, the model already includes solvent entropic contributions implicitly, so entropy calculations are likely to be overestimated. Secondly, the model neglects solute–solvent interactions, meaning large errors may be introduced due to neglect of low frequency vibrational modes. To overcome these deficiencies, the calculation is divided into two parts. The first involves determination of the gas-phase reaction free energies of electron attachment ($\Delta G_{EA}(g)$) by calculation of the changes in enthalpy (H) and entropy (S) for each of the species involved in the reaction (eqn (1)). The solvation free energy change (ΔG_{solv}) of a species is obtained as the energy difference between the gas-phase SCF energy given in appropriate units (E_{ZPE}), calculated at the gas-phase geometry, and the total free energy of the solvated species at the relaxed solvated geometry. Since the IEFPCM model implicitly includes solvent entropic contributions, this provides a good estimate for the true value of ΔG_{solv}.[18]

$$\Delta G_{EA}(g) = \Delta H - T\Delta S \quad (1)$$

Table 2 contains all the thermodynamic variables calculated for each species of interest. Individual gas-phase free energies are not shown, since they have little meaning until compared with one another. The interplay between solvation free energies and the charge on each species is interesting to note. The neutral species favour solvation in the low dielectric solvent (*i.e.*, CH_2Cl_2), while doubly charged species (either positively or negatively charged) exhibit a greater stabilisation in CH_3CN. For singly charged species, it seems that low polarity is favoured.

A complete model of the reduction of **1** requires knowledge of the acidity constants for each species. The accurate determination of a pK_A value by computational methods is a particularly difficult undertaking,[19] and relies to a great extent on the quality of the reference used to model the solvated proton.[20] In many cases, the experimental value for a solvated proton is used.[21] However, in the present case, where the solvents under investigation are non-aqueous, such a value is not well defined. Instead, we have elected to model the solvated proton explicitly as a protonated H_8O_4–$H_9O_4^+$ cluster, with the non-protonated cluster acting as the reference.[22] This cluster was found to be the smallest system able to provide reasonable results in aqueous calculations. It should be recalled that pK_A values obtained using by this method are not absolute, but are relative to water in the same environment.

Table 2 Computed energies and thermodynamic parameters for all species considered here

Species	E_{SCF} (Hartree)	$E_{ZPE}{}^a$	H^a	S^b	$\Delta G_{Solv}{}^{ac}$	$\Delta G_{Solv}{}^{ad}$
S	−1258.51	428	458	425	−33	2
HS^+	−1258.83	454	485	429	−163	−141
H_2S^{2+}	−1258.99	475	508	444	−535	−555
$R^{-\bullet}$	−1258.56	421	453	444	−182	−167
$RH^\bullet$	−1259.08	446	480	478	−21	15
$RH_2^{+\bullet}$	−1259.43	471	506	471	−120	−120
T^{2-}	−1258.52	417	449	449	−626	−659
TH^-	−1259.18	441	473	443	−184	−171
TH_2	−1259.71	469	505	478	−27	8

[a] Units of kJ mol^{-1}. [b] Units of J K^{-1} mol^{-1}. [c] CH_2Cl_2. [d] CH_3CN.

Now, the pK_A may be determined from the solvated free-energy of protonation, $\Delta_{dp}G^0_{(sol)}$, on the basis of eqn (2).

$$pK_A = \frac{\Delta_{dp}G^0_{(sol)}}{2.303\ RT} \quad (2)$$

In determining $\Delta_{dp}G^0_{(sol)}$, we have separated the calculation into gas-phase and solvation terms. Eqn (3) and eqn (4) show how the free-energy of deprotonation in the gas phase, $\Delta_{dp}G^0_{(gas)}$, and individual solvent free-energies of solvation, $\Delta_{solv}G^0(X)$, are combined to calculate $\Delta_{dp}G^0_{(sol)}$.[23]

$$\Delta_{dp}G^0_{(sol)} = \Delta_{dp}G^0_{(gas)} + \Delta_{solv}G^0(A) - \Delta_{solv}G^0(AH^+) + \Delta_{solv}G^0(H^+) \quad (3)$$

$$\Delta_{solv}G^0(H^+) = \Delta_{solv}G^0(H_9O_4^+) - \Delta_{solv}G^0(H_8O_4) \quad (4)$$

Table 2 contains the results of these calculations, as applied to the protonation steps illustrated in Scheme 2. For all pathways considered, protonation of a neutral species to form the conjugate acid is unfavourable, as indicated by the negative pK_A for that step. However, the data indicate that the π-radical anion is susceptible to protonation (pK_A = 8.4), giving RH•, if a source of protons is available. The dianion, T^{2-}, is likely to be protonated in any medium (pK_A = 20.4) while formation of the di-protonated species, TH_2, is also favourable (pK_A = 13.8).

Molecular dynamics simulations

To further investigate the protonation/geometry change, we have performed molecular dynamics simulations (MDS) on the various species. Since the processes of interest involve electron addition and bond breaking, molecular mechanics methods, as commonly used for dynamics simulations, are inappropriate. Therefore, we have used the semi-empirical MOPAC method[24] encoded within the CHARMM dynamics environment.[25] Three separate sets of trajectories were calculated, one for each of the possible states of **1** and, at intervals of 100 ps, an electron is added to the simulation in order to reduce the solute. The dihedral angle is monitored throughout the simulation as a means by which to gauge the scale of geometric distortion, and Fig. 7 shows the results for all species. Starting with the neutral form of **1**, which we believe to be the only species present at the onset of experiment (left panel of Fig. 7), the initial phase of the trajectory (*i.e.*, 0–100 ps) exhibits simple oscillation of the dihedral angle around the minimum. The mean value for the dihedral angle during this phase is 27°, in reasonable agreement with the minimum energy value of 33°. However, upon addition of the first electron (*i.e.*, 100–200 ps), there is a slight reduction in the mean value of the dihedral angle to 22°. This is contrary to both the geometry optimised structures and chemical intuition, and demonstrates the weakness of the method. On addition of a second electron, producing the T^{2-}, the calculation fails to reach SCF convergence.

For both HS^+ and H_2S^{2+}, these being hypothetic structures, the initial phase of the MDS proceeds as described for S, with mean dihedral angles of 29° and 28°, respectively. Addition of the first electron has a profound effect on both these two structures. Thus, for SH•, there is a near instantaneous change in geometry to a mean dihedral angle of 97°, in agreement with the minimum energy structure calculated in Table 1. Furthermore, the new potential surface allows for a much wider scale of motion such that the standard deviation of the dihedral angle is 24.9°. This indicates that the S–S bond has been broken. Addition of the second electron at 200 ps decreases the dihedral angle, effectively reforming the bridge. In this state, the mean dihedral angle is 58°, which remains in excellent agreement with the previously calculated value. Furthermore, the single proton positions itself between the two sulfur atoms in the manner predicted by the minimum energy calculations. A particularly interesting feature of this species is that the proton bridge is surprisingly rigid; the standard deviation of the dihedral angle computed for TH^- is only 7.1°.

The MDS runs made for the di-protonated species shows that the S–S is broken concomitantly with addition of the first electron (Fig. 7). A mean dihedral angle of 140° is calculated for the reduced species, $H_2R^{+\bullet}$. There is a surprising rigidity,

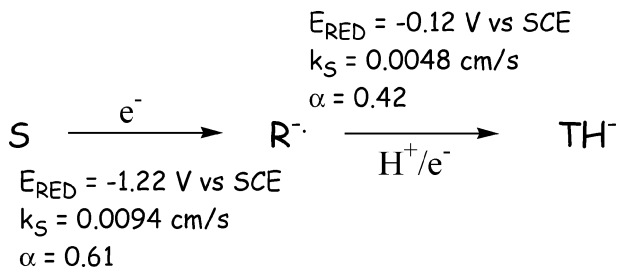

Scheme 2 Main pathway for the two-electron reduction of **1** in CH_2Cl_2 with the electrochemical data obtained from simulation of the cyclic voltammograms recorded at room temperature.

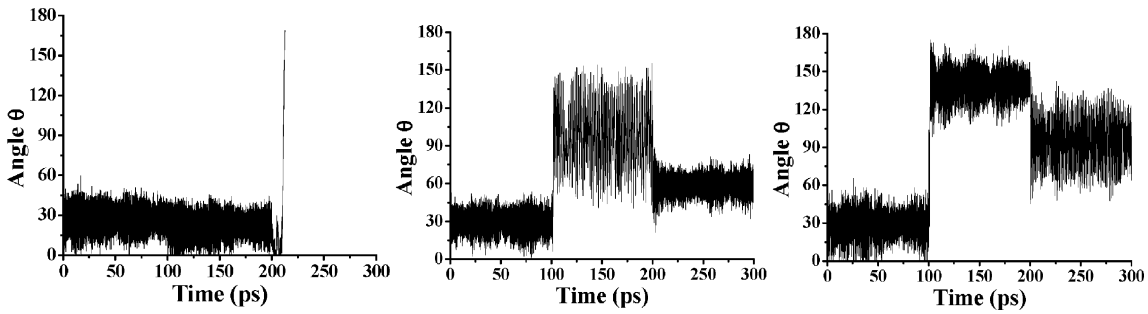

Fig. 7 Results of MDS runs carried out for the unprotonated species (left), the mono-protonated molecule (centre) and the di-protonated solute (right). Single electrons are injected after 100 ps and after 200 ps in each case.

with the standard deviation being 14.2°, when we might have expected the dihedral angle to show similar flexibility to that of RH•, and at the present time the reason for this apparent constraint is unclear. Addition of the second electron, forming the neutral species TH_2, causes the adoption of a near perpendicular geometry, as predicted by the DFT calculations.

Calculation of reduction potentials

Combining the information listed in Table 1 and Table 2 indicates that we need consider only the neutral species S at the beginning of the experiment. The final product will be either TH^- or possibly TH_2. Both these latter species lack the S–S bond, according to both the MDS runs and the computed lowest-energy structures. The intermediate species is subject to protonation, forming RH• as the most likely species, but there seems little chance of forming the di-protonated species $RH_2^{+\bullet}$. The stage is now set to compute the respective reduction potentials, using the well-known relationship between free energy and reduction potential (eqn (5)), where the number of electrons, n, is unity in all cases.

$$\Delta G^0_{(sol)} = -nF\Delta E^0 \qquad (5)$$

Reduction potentials obtained in this way are absolute,[26] and as such must be made relative to an experimental electrode before use.[27] This is easily achieved by subtraction of 4.189 V from the final result. This value is based on the experimentally determined absolute value of the hydrogen electrode minus the standard potential of the calomel electrode (0.241 V).[18] Table 3 contains the calculated reduction potentials for significant electrode reactions described in Scheme 1. Firstly, we consider the values computed in the absence of a proton source.[29] In agreement with the experimental studies, addition of the first electron requires a strongly cathodic potential. The computed E_{RED} values are somewhat different for the two solvents, with reduction being easier in CH_3CN. Addition of the second electron is subject to potential inversion in both solvents, although the reduction potentials for the second step are quite different. Again, the polar solvent appears to assist reduction to the anionic product. Indeed, the extent of potential inversion is pronounced in CH_3CN solution. The π-radical anion formed during the first reduction step, $R^{-\bullet}$, is possibly protonated in the presence of a suitable proton source. The MDS runs indicate that this might be a fast process, although it is unlikely that it will compete with further reduction during cyclic voltammetry. The quantum chemical calculations show that E_{RED} for the protonated species, RH•, is slightly positive in both solvents. This situation serves to enhance the degree of potential inversion and means that the first reduction product is highly susceptible to further reduction. It is considered unlikely that $RH_2^{+\bullet}$ will be formed in an organic solvent while the computational studies suggest that this species is very easily reduced.

Data simulation

The cyclic voltammograms recorded in CH_2Cl_2 at room temperature were subjected to computer simulation, on the basis of two successive one-electron-transfer steps, each with an associated reduction potential, E_{RED}, a characteristic electrochemical rate constant, k_S, and a transfer coefficient, α.[30] The diffusion coefficient was kept fixed at the value measured earlier. Simulations were carried out for all sweep rates covered experimentally and the averaged parameters are given in terms of Scheme 2. Simulations were made for two solute concentrations. In order to obtain an adequate representation of the experimental voltammogram it was necessary to add a proton during the second reduction step. The entire cyclic voltammogram was simulated, not just the cathodic wave. Within these conditions, good fits to the experimental curves could be generated using reasonable values for the various parameters. A typical comparison of the experimental and simulated cyclic voltammograms recorded for the reduction of **1** at a sweep rate of 2 V s^{-1} and at 20 °C is shown as Fig. 8.

Thus, the one-electron reduction of **1** in CH_2Cl_2 proceeds smoothly to give the corresponding π-radical anion. There is a modest structural change accompanying this reduction step but no concomitant protonation of the resultant π-radical anion. Data simulation estimates the one-electron reduction potential to be −1.22 V *vs.* SCE under these conditions, while the transfer coefficient is computed to be 0.61. It is notable that the derived E_{RED} is in remarkably good agreement with that computed by the quantum chemical approach, where E_{RED} = −1.16 V *vs.* SCE. The electrochemical rate constant, k_S, is calculated to be 0.0094 cm s^{-1}. This seems to be a reasonable value in light of the moderate geometrical change that follows from addition of the first electron. The simulation requires that the second reduction step is seriously inverted since E_{RED} is derived to be −0.12 V *vs.* SCE. In fact, this situation corresponds to potential inversion of 1.04 V. For the second step, α = 0.42 and k_S is calculated to be 0.0048 cm s^{-1}. Again, these parameters seem quite reasonable and fully consistent with the proposed mechanism. The quantum chemical studies indicate E_{RED} values of 0.22 and −0.76 V *vs.* SCE, respectively, with and without protonation. Slightly better agreement is reached for the case where the relaxed π-radical anion, $R^{-\bullet}$, is reduced to the dithiolate and simultaneously

Table 3 Computed thermodynamic parameters for the various redox steps of interest; units being given as kJ mol^{-1} unless stated otherwise

Species[a]	ΔG_{EA}(gas)	$\Delta\Delta G_{Solv}$[b]	$\Delta\Delta G_{Solv}$[c]	ΔG_{EA}[b]	ΔG_{EA}[c]	E_{RED}[bd]	E_{RED}[cd]
S	−142	−150	−169	−292	−312	−1.16	−0.96
HS^+	−662	142	157	−520	−505	1.20	1.05
H_2S^{2+}	−1171	415	435	−756	−736	3.65	3.44
$R^{-\bullet}$	112	−443	−492	−331	−379	−0.76	−0.26
RH•	−262	−164	−186	−425	−448	0.22	0.45
$RH^{+\bullet}$	−729	93	128	−636	−601	2.40	2.04

[a] Refers to the starting species prior to addition of one electron. [b] Refers to CH_2Cl_2. [c] Refers to CH_3CN. [d] Units of V *vs.* SCE.

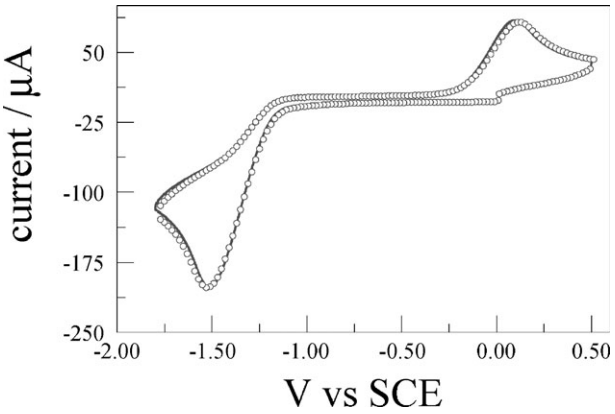

Fig. 8 Comparison of experimental cyclic voltammogram (solid line) and simulated curve (open circles) for **1** in CH_2Cl_2. The sweep rate was 2 V s^{-1}.

protonated to give TH^-. Here, the computed E_{RED} is 0.14 V *vs.* SCE. The overall fit to the experimental record is vastly improved by inclusion of this single protonation step and we consider that this represents the actual situation.

Electrostatic interactions

Both the experimental and theoretical results agree that the second step of the two-electron reduction of **1** occurs at a less negative potential than the first. There are relatively few examples in the literature of such behaviour,[31] and all involve species undergoing significant structural alteration, thereby significantly changing the environment. The extent to which **1** might achieve such distortion appears, at first glance, to be limited. The only major geometry change that occurs upon reduction is an increase in the central dihedral angle. This structural change is driven by the need to reduce the extent of electrostatic repulsion. To show this, we have calculated the partial charges for the various species in the absence of protonation. These partial charges are then used to compute the electrostatic interaction energy for the singly- and doubly-reduced species, using eqn (6), the energy being calculated in terms of the distance between point charges.[32]

$$E = \frac{1}{4\pi\xi_0}\sum_i^n\sum_j^n\frac{q_i q_j}{r_{ij}} \qquad (6)$$

Here, ξ_0 is the permittivity of free space and q_i and q_j are the partial charges of atoms i and j, separated by a distance of r_{ij}. We find that the total electrostatic energy is -214 kJ mol^{-1} for the neutral species, S, -15 kJ mol^{-1} for $R^{-\bullet}$, and -102 kJ mol^{-1} for T^{2-}. Thus, despite having doubled the negative charge, cleaving the S–S bond is sufficient to significantly reduce the electron repulsion. Mono-protonation of the dithiolate product serves to further reduce the electrostatic energy, despite bringing the sulfur centres into closer proximity.

Concluding remarks

This research has been concerned with the design and critical examination of a small molecular system intended to store information on a transient basis. Although, in principle, the system could be activated by thermal, photochemical or electrochemical stimulation, because of inherent limitations, our attention has been restricted to an electrochemical cycle. Here, the writing process is achieved by application of a cathodic potential whilst the erase step consists of applying a suitable anodic potential. The study involves three interlocked components; namely, electrochemical measurements, theoretical modelling to better understand the mechanism, and mathematical simulation to resolve the potential inversion characteristics. The key feature of the work relates to the large-scale geometrical changes that accompany the electrochemical steps. An essential feature of the long-term stability of the system involves seeking a detailed understanding of protonation of the anionic species formed upon one- or two-electron reduction of the disulfide. This latter situation has important implications for the reduction potentials and stabilities of the products.

Reduction of the disulfide is a two-electron process. Both experimental and theoretical studies point towards potential inversion whereby addition of the second electron occurs at a less negative potential than that needed to effect attachment of the first electron.[16,31] The underlying reason behind such behaviour stems from the structural changes that accompany one-electron reduction. Thus, the anion radical possesses an extended S–S bond but this remains intact. The extra electron is located primarily in the σ* orbital associated with the S–S bond. Protonation affects the structure of this species. Moreover, the S–S bond cleaves upon addition of the second electron and the resultant thiolate anions move apart to escape electrostatic repulsion. The entire process is reversed on application of an anodic potential. It is important to stress that many redox cycles can be achieved without loss of activity or current. The amount of chemical change is easily quantified by measuring the current.

Our computational studies have addressed the role of protonation of the dithiolate product. For effective memory storage, the final product must be highly stable and unaffected by closing down the circuitry. In this respect, the dithiol has certain advantages over the corresponding dithiolate. Experimental studies have confirmed that the product is stable over several days at ambient temperature and that the memory cycle can be completed after storing a partially electrolysed solution for more than one week. Molecular oxygen affects the cathodic process but not the subsequent reversal. There is only a modest nuclear reorganisation energy associated with formation of the anion radical, somewhere in the region of 0.3 eV as determined by comparing all the changes in bond length upon addition of the electron. The reorganisation energy is increased dramatically for formation of the dithiolate, and a value of around 1 eV is obtained from the structural data. Interestingly, the mono-protonated species, TH^-, is associated with the more modest reorganisation energy of 0.57 eV since the structural change is less pronounced than for formation of the dianion. Since a proton source could be incorporated into the overall system, it should be possible to drive the chemistry towards TH^- or indeed TH_2.

The quantum chemical studies are strongly supportive of potential inversion and it has not been possible to analyse the experimental data without allowing for this feature. Protonation of the dithiolate enhances the disparity between the two

reduction potentials and also minimises the extent of the geometric change that accompanies the addition of the second proton. The computational work indicates that the attached proton resides midway between the sulfur atoms and has the appearance of a bridge. Even so, the S–S distance of 3.4 Å is too long to support a formal bond. Agreement between calculated and experimental reduction potentials is remarkably good. Given that calculation of reduction potentials can be highly challenging, this agreement is extremely rewarding and opens the way to using quantum chemistry as a design element for next-generation prototypes.

In terms of a practical device, we note firstly that a second disulfide residue could be added to the switch centre.[33] This would raise the number of stored electrons from two to four for each molecule. Secondly, small oligomers could be synthesised by joining successive molecules into linear or branched arrays so that multi-electron storage becomes possible. There are no accompanying colour changes so the system should not be considered as an electrochromic (or indeed electro-luminescent) device. Attaching the molecule to an electrode should be straightforward and, in principle, a very high density of molecules, each capable of storing many electrons, could be engineered. The system described here provides for high-density DRAM and is suitable for 3D recording. It has the capability for non-volatile memory storage at the molecular level. Miniaturised systems could be built by replacing one of the macroscopic electrodes with the tip of a scanning electrochemical microscope so that spatial resolution becomes possible.

The remaining question to be addressed relates to how best to read the stored information without perturbing the system. Surface-enhanced spectroscopic techniques, such as total internal reflection infrared or resonance Raman, offer many possibilities to monitor the structural changes. These techniques are fast and reliable. A simpler approach involves attaching a fluorophore to the disulfide such that reduction switches on fluorescence. We have made some progress along these lines and have been able to induce fluorescence modulation by switching the redox state of the attached disulfide.[10] Likewise, work is in progress aimed at equipping the system with a chemical means for encoding and decoding information at the molecular level. Such features represent the next stage of development.

Experimental

Methods and materials

All chemicals were purchased from Aldrich Chemicals Co. and were used as received. The starting material 4,4′-diiodobiphenyl-2,2′-diol was prepared following a literature method.[33] Solvents were dried by standard procedures before being distilled and stored under nitrogen over 4 Å molecular sieves.[34] ^{1}H and ^{13}C NMR spectra were recorded with a Bruker AVANCE 300 MHz spectrometer. EPR studies were conducted at the EPSRC-sponsored EPR Centre at the University of Manchester. Routine mass spectra and elemental analyses were obtained using in-house facilities. Spectroscopic grade solvents were obtained from Aldrich Chemical Co. and were redistilled before use. The procedure used for preparation of compound **1** is shown in Scheme 3.

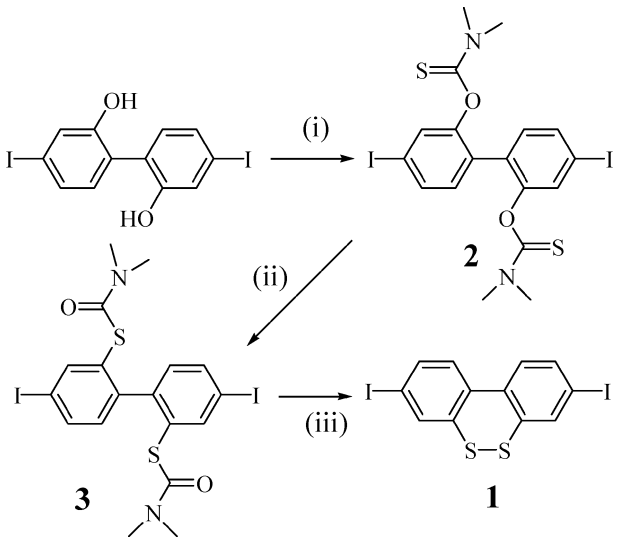

Scheme 3 Reagents and conditions: (i) NaH, DMF, Me_2NCSCl, 85 °C; (ii) 200 °C, 6 h; (iii) NaOH, THF–MeOH, 30 min.

Synthesis

Dimethylthiocarbamic acid *O*-(2′-dimethylthiocarbamoyloxy-4,4′-diiodobiphenyl-2-yl) ester (2). A solution of 4,4′-diiodobiphenyl-2,2′-diol (0.8 g, 1.8 mmol) in dry DMF (100 mL) containing NaH (0.22 g, 5.49 mmol) was stirred under N_2 at room temperature for 2 h. During this time the colour of the solution changed from brown to beige. An aliquot of Me_2NCSCl (0.69 g, 5.49 mmol) was added and the mixture heated at 85 °C for 2 h. Afterwards the mixture was cooled to room temperature and stirred overnight. Aqueous KOH (2% w/w) was added and the resultant white precipitate was extracted with CH_2Cl_2 (3 × 50 mL). The combined organics were dried over $MgSO_4$, filtered, and removed on a rotary evaporator to afford the crude product. This material was purified on silica gel using petroleum ether–Et_2O (2 : 1) as eluent to afford a white solid. Yield 0.8 g, 1.83 mmol, 70%. ^{1}H NMR (300 MHz, $CDCl_3$): δ = 7.59 (dd, 2H, J = 8.0 Hz, J' = 1.7 Hz), 7.53 (d, 2H, J = 1.7 Hz), 7.12 (d, 2H, J = 8.0 Hz), 3.30 (s, 6H), 3.09 (s, 6H). ^{13}C NMR (75.5 MHz, $CDCl_3$) δ = 186.8, 151.6, 135.1, 133.5, 132.8, 130.2, 93.1, 43.7, 39.1. EI-MS (m/z): calc. for $C_{18}H_{18}I_2N_2O_2S_2$ 611.8899, fnd 611.8919. M.p: 200–202 °C. Elemental analysis: calc. (fnd) for $C_{18}H_{18}I_2N_2O_2S_2$ C, 35.51 (35.23), H, 2.96 (2.96), N, 4.58 (4.41).

Dimethylthiocarbamic acid *S*-(2′-dimethylcarbamoylsulfanyl-4,4′-diiodobiphenyl-2-yl) ester (3). A 100 ml round-bottomed flask was charged with **2** (300 mg, 5 mmol) and fitted with an air condenser. The flask was put under a positive pressure of N_2 and heated in an oil bath at 200 °C for 6 h. The mixture was cooled to room temperature and the resultant slurry taken up in CH_2Cl_2 (100 mL) and filtered to remove insoluble material. Evaporation of the organic solvent afforded a crude mixture which was purified by column chromatography on silica gel using petroleum ether–Et_2O (1 : 1) as eluent. Recrystallisation

of the isolated residue from Et_2O afforded the desired product as a white solid. Yield 120 mg, 0.2 mmol, 40%. ^{1}H NMR (300 MHz, $CDCl_3$) δ = 7.93 (d, 2H, J = 1.8 Hz), 7.71 (dd, 2H, J = 8.1 Hz, J' = 1.8 Hz), 7.00 (d, 2H, J = 8.1 Hz). ^{13}C NMR (75.5 MHz, $CDCl_3$) δ = 145.5, 137.6, 133.2, 130.6, 127.3, 123.6, 92.5, 92.0, 40.6. M.p: 190–192 °C. EI-MS (m/z): calc. for $C_{18}H_{18}I_2N_2O_2S_2$ 612.3, fnd 612.0. Elemental analysis: calc. (fnd) for $C_{18}H_{18}I_2N_2O_2S_2$ 35.51 (35.40), H, 2.96 (2.98), N, 4.58 (4.62).

3,8-Diiododibenzo[1,2]dithiine (1). Compound **3** (80 mg, 0.13 mmol) was dissolved in dry THF (10 mL) and MeOH (5 mL) and purged with N_2. The solution was brought to reflux and a solution of NaOH (20 mg, 0.5 mmol) in MeOH (5 mL) was added. The mixture was refluxed for 30 minutes and cooled to room temperature. Water (10 mL) was added and the solution acidified with conc. H_2SO_4 to afford a white precipitate that was extracted into Et_2O (50 mL). The organic solvent was dried over $MgSO_4$, filtered and removed on a rotary evaporator. The crude product was purified by column chromatography on silica gel using petroleum ether–Et_2O (3 : 1) as eluent. Recrystallisation of the product from $CHCl_3$ afforded the desired product as a yellow solid. Yield 50 mg, 0.1 mmol, 80%. ^{1}H NMR (300 MHz, $CDCl_3$) δ = 7.85 (d, 2H, J = 1.8 Hz), 7.69 (dd, 2H, J = 8.3 Hz, J' = 1.8 Hz), 7.35 (d, 2H, J = 8.3 Hz). ^{13}C NMR (75.5 MHz, $CDCl_3$) δ = 138.4, 138.1, 137.7, 137.2, 129.0, 94.0. M.p: 150–152 °C. EI-MS (m/z): calc. for $C_{12}H_6I_2S_2$ 467.8000, fnd 467.8006. Elemental analysis: calc. (fnd) for $C_{12}H_6I_2S_2$ 30.79 (29.42), H, 1.29 (1.08).

Electrochemical methods

Cyclic voltammetry studies were carried out in dried CH_2Cl_2 containing 0.2 M tetra-*N*-butylammonium hexafluorophosphate, freshly recrystallised, as background electrolyte using a conventional three-electrode cell. Solutions of the solute (*ca.* 1 mM) were purged thoroughly with N_2 prior to electrolysis and the solvent was distilled immediately before use. The working, counter and reference electrodes were glassy carbon, platinum wire and Ag/AgCl, respectively. The cell was controlled with a HCH Instruments Electrochemical Analyzer connected to a PC running CHI600 software and was maintained at 20 °C. Prior to making measurements the working electrode was polished to a mirror shine using an alumina slurry made up with deionised water. The reference electrode was stored in 3 M KCl solution to prevent the electrode from drying out and was calibrated using ferrocene as internal standard. The glassware was cleaned by sonication in a detergent solution containing Decon-90 followed by thorough rinsing with conductivity water. The cell was dried in the oven to remove residual moisture. Where appropriate, the sample cell was housed in a Faraday cage to minimise RF disturbance of the signal. Computer simulations were made using DigiElch.

Spectroelectrochemistry was carried out using a Spec-Ac optically-thin, transparent electrode (OTTEL) cell mounted in a Perkin-Elmer UV/visible spectrophotometer. The working electrode was a fine platinum mesh situated in the path of the absorption beam. Counter and reference electrodes were both platinum wire. The potential of the cell was controlled using the HCH Instruments Electrochemical Analyzer networked to a computer running CHI600 software. EPR studies were conducted using *in situ* electrochemical reduction of the sample. These studies were carried out at the EPSRC-funded National EPR Service at the University of Manchester. The cell is essentially a modified flat cell containing three electrodes; an Ag/AgCl reference electrode, a platinum wire counter electrode and a platinum mesh working electrode located in the thin section of the cell. Solutions were made up in CH_2Cl_2 (*ca.* 1 mM) containing 0.1 M tetra-*N*-butyl ammonium tetrafluoroborate as background electrolyte and were rigorously de-oxygenated prior to transfer to the cell under a nitrogen atmosphere. The sample was then placed in the cavity of the spectrometer (Bruker EMX running at X-Band) and reduced at the appropriate voltage (using values measured from prior cyclic voltammetric studies). The cell was carefully positioned, so that the mesh electrode, where reduction was to take place, was centred in the cavity. The potential was controlled using an Autolab potentiostat controlled by a laptop PC running General Purpose Electrochemical System version 4.9.

Initial geometry optimisations for all thermodynamics calculations were performed using GAMESS,[35] with the B3LYP DFT method and the 6-31+G* basis set. The geometries for all structures were then re-optimised using the Gaussian-03 program,[36] at the B3LYP/6-31++G** level, while thermodynamic properties were also determined at this level. Vibrational frequencies were also calculated to ensure global minimum structures were obtained. Solvent effects were determined using the IEFPCM method as implemented in Gaussian-03. Molecular dynamics trajectories were determined using the MOPAC semi-empirical package,[24] implemented within the CHARMM molecular dynamics system.[25] For all trajectories, an initial heating step of 50 ps raises the temperature of the system from 0 to 298 K. An equilibration period of 100 ps was then followed by a 'production run' of 100 ps. This latter step constitutes the results for the neutral species. The charge in the system was then decremented (*i.e.*, an electron was added) and the simulation was allowed to continue for a further 100 ps. A second electron was added and a further 100 ps trajectory was recorded. Bond lengths and bond angles were taken from the computed structures.

Acknowledgements

We thank the EPSRC (EP/C007727/1) and University of Newcastle for financial support of this work. The EPR studies were made at the EPSRC-sponsored EPR Centre at the University of Manchester.

References

1 A. A. Sirenko, C. Bernhard, A. Golnik, A. M Clark, J. H. Hao, W. D. Si and X. X. Xi, *Nature*, 2000, **404**, 373; S. K. Kim, G.-J. Choi, S. Y. Lee, M. Seo, S. W. Lee, J. H. Han, H.-S. Ahn, S. Han and C. S. Hwang, *Adv. Mater.*, 2008, **20**, 1429.
2 E. A. Weiss, M. R. Wasielewski and M. A. Ratner, *Top. Curr. Chem.*, 2005, **257**, 103.
3 J. E. Green, J. W. Choi, A. Boukai, Y. Bunimovich, E. Johnston-Halperin, E. DeIonno, Y. Luo, B. A. Sheriff, K. Xu, Y. S. Shin, H.-R. Tseng, J. F. Stoddart and J. R. Heath, *Nature*, 2006, **445**, 414.

4 C. Li, B. Lei, W. Fan, D. Zhang, M. Meyyappan and C. Zhou, *J. Nanosci. Nanotechnol.*, 2007, **7**, 138.
5 R. Beckman, K. Beverly, A. Boukai, Y. Bunimovich, J. W. Choi, E. Delonno, J. Green, E. Johnston-Halperin, Y. Luo, B. Sheriff, J. F. Stoddart and J. R. Heath, *Faraday Discuss.*, 2006, **131**, 9.
6 H. Mustroph, M. Stollenwerk and V. Bressau, *Angew. Chem., Int. Ed.*, 2006, **45**, 2016.
7 C. Li, W. Fan, N. Lei, D. Zhang, S. Han, T. Tang, X. Liu, Z. Liu, A. Asano, M. Meyyappan, J. Han and C. Zhou, *App. Phys. Lett.*, 2004, **84**, 1949.
8 J. He, F. Chen, P. A. Liddell, J. Andréasson, S. D. Straight, D. Gust, T. A. Moore, A. L. Moore, J. Li, O. F. Sankey and S. M. Lindsay, *Nanotechnology*, 2005, **16**, 695.
9 B. Persson, *J. Electroanal. Chem.*, 1978, **86**, 313; F. Mango, G. Bontempelli and G. Pilloni, *J. Electroanal. Chem.*, 1971, **30**, 375; T. B. Christensen and K. Daasbjerg, *Acta Chem. Scand.*, 1997, **51**, 307; M. Liu, S. J. Visco and L. C. De Jonghue, *J. Electrochem. Soc.*, 1989, **136**, 2570; S. Antonello, K. Daasbjerg, H. Jensen, F. Taddei and F. Maran, *J. Am. Chem. Soc.*, 2003, **125**, 14905; K. Daasbjerg, H. Jensen, R. Benassi, F. Taddei, S. Antonello, A. Gennaro and F. Maran, *J. Am. Chem. Soc.*, 1999, **121**, 1750; A. Houmam, *Chem. Rev.*, 2008, **108**, 2180.
10 I. Llarena, A. C. Benniston, G. Izzet, D. B. Rewinska, R. W. Harrington and W. Clegg, *Tetrahedron Lett.*, 2006, **47**, 9135.
11 A. J. Bard and L. R. Faulkner, *Electrochemical Methods: Fundamentals and Applications*, Wiley, New York, 1980; C. Costentin, M. Robert and J.-M. Savéant, *Chem. Phys.*, 2006, **324**, 40; C. Costentin, M. Robert and J.-M. Savéant, *J. Am. Chem. Soc.*, 2004, **126**, 16834; L. Pause, M. Robert and J.-M. Savéant, *J. Am. Chem. Soc.*, 2001, **123**, 4886.
12 H. Ikeuchi, *J. Electroanal. Chem.*, 2005, **577**, 55.
13 D. Shoup and A. Szabo, *J. Electroanal. Chem.*, 1982, **140**, 237.
14 J.-M. Savéant, *J. Am. Chem. Soc.*, 1987, **109**, 6788.
15 E. Gileadi, *J. Electroanal. Chem.*, 2002, **532**, 181.
16 N. E. Gruhn, N. A. Marcía-Ruvalcaba and D. H. Evans, *Langmuir*, 2006, **22**, 10683.
17 E. Cancès, B. Mennucci and J. Tomasi, *J. Chem. Phys.*, 1997, **107**, 3032.
18 J. P. Holland, J. C. Green and J. R. Dilworth, *Dalton Trans.*, 2006, 783.
19 H. Lu, X. Chen and C. G. Zhan, *J. Phys. Chem. B*, 2007, **111**, 10599.
20 J. R. Pliego, *Chem. Phys. Lett.*, 2003, **367**, 145; G. I. Almerindo, D. W. Tondo and J. R. Pliego, *J. Phys. Chem. A*, 2004, **108**, 166; J. N. Li, Y. Fu, L. Liu and Q. X. Guo, *Tetrahedron*, 2006, **62**, 11801.
21 G. A. A. Saracino, R. Improta and V. Barone, *Chem. Phys. Lett.*, 2003, **373**, 411.
22 J. R. Pliego and J. M. Riveros, *J. Phys. Chem. A*, 2002, **106**, 7434.
23 D. H. Evans and K. Hu, *J. Chem. Soc., Faraday Trans.*, 1996, **92**, 3983.
24 Molecular Orbital PACkage (J. J. P. Stewart and Fujitsu Limited. Copyright Fujitsu Limited, Tokyo, Japan).
25 B. R. Brooks, R. E. Burccoleri, B. D. Olafson, D. J. States, S. Swaminathan and M. Karplus, *J. Comput. Chem.*, 1983, **4**, 187.
26 P. Winget, C. J. Cramer and D. G. Truhlar, *Theor. Chem. Acc.*, 2004, **112**, 2004.
27 D. T. Sawyer, A. Sobkowiak and J. L. Roberts, *Electrochemistry for Chemists*, Wiley-Interscience, New York, 2nd edn, 1995.
28 N. A. Marcía-Ruvalcaba and D. H. Evans, *J. Phys. Chem. B*, 2006, **110**, 5155.
29 N. Mehta and S. N. Datta, *J. Chem. Phys. B*, 2007, **111**, 7210; M. H. Baik, J. S. Silverman, I. V. Yang, P. A. Ropp, V. A. Szalai, W. Yang and H. H. Thorp, *J. Phys. Chem. B*, 2001, **105**, 6437; S. N. Datta, J. Sudhamsu and A. Pandey, *J. Phys. Chem. B*, 2004, **108**, 8007; P. Jaque, A. V. Marenich, C. J. Cramer and D. G. Truhlar, *J. Phys. Chem. C*, 2007, **111**, 5783.
30 D. H. Evans and M. W. Lehmann, *Acta Chem. Scand.*, 1999, **53**, 765.
31 S. Cossu, O. De Lucchi, E. Piga and G. Valle, *Phosphorus, Sulfur Silicon Relat. Elem.*, 1991, **63**, 51; Q. Zhi-Ohlback, R. Gletier, F. Rominger, H.-L. Schmidt and R. Reda, *Eur. J. Org. Chem.*, 1998, 2409.
32 G. C. Hall, *Int. J. Quantum Chem.*, 2004, **16**, 51.
33 A. C. Benniston, P. Li and C. A. Sams, *Tetrahedron Lett.*, 2003, **44**, 3947; A. C. Benniston, A. Harriman, P. Li, P. V Patel and C. A. Sams, *J. Org. Chem.*, 2006, **71**, 3481.
34 W. L. F. Armarego and C. L. L. Chai, *Purification of Laboratory Chemicals*, Butterworth-Heineman, London, 2003, 5th edn.
35 GAMESS-UK is a package of *ab initio* programs. See: "http://www.cfs.dl.ac.uk/gamess-uk/index.shtml" M. F. Guest, I. J. Bush, H. J. J. van Dam, P. Sherwood, J. M. H. Thomas, J. H. van Lenthe, R. W. A Havenith and J. Kendrick, "The GAMESS-UK electronic structure package: algorithms, developments and applications", *Molecular Physics*, 20 March–20 April 2005, **103**(6–8), 719–747.
36 M. J. Frisch, G. W. Trucks, H. B. Schlegel, G. E. Scuseria, M. A. Robb, J. R. Cheeseman, J. A. Montgomery, Jr, T. Vreven, K. N. Kudin, J. C. Burant, J. M. Millam, S. S. Iyengar, J. Tomasi, V. Barone, B. Mennucci, M. Cossi, G. Scalmani, N. Rega, G. A. Petersson, H. Nakatsuji, M. Hada, M. Ehara, K. Toyota, R. Fukuda, J. Hasegawa, M. Ishida, T. Nakajima, Y. Honda, O. Kitao, H. Nakai, M. Klene, X. Li, J. E. Knox, H. P. Hratchian, J. B. Cross, V. Bakken, C. Adamo, J. Jaramillo, R. Gomperts, R. E. Stratmann, O. Yazyev, A. J. Austin, R. Cammi, C. Pomelli, J. W. Ochterski, P. Y. Ayala, K. Morokuma, G. A. Voth, P. Salvador, J. J. Dannenberg, V. G. Zakrzewski, S. Dapprich, A. D. Daniels, M. C. Strain, O. Farkas, D. K. Malick, A. D. Rabuck, K. Raghavachari, J. B. Foresman, J. V. Ortiz, Q. Cui, A. G. Baboul, S. Clifford, J. Cioslowski, B. B. Stefanov, G. Liu, A. Liashenko, P. Piskorz, I. Komaromi, R. L. Martin, D. J. Fox, T. Keith, M. A. Al-Laham, C. Y. Peng, A. Nanayakkara, M. Challacombe, P. M. W. Gill, B. Johnson, W. Chen, M. W. Wong, C. Gonzalez and J. A. Pople, *GAUSSIAN 03 (Revision C.02)*, Gaussian, Inc., Wallingford, CT, 2004.